Structure of MlaFEDB lipid transporter reveals an ABC exporter fold and two bound phospholipids

Nicolas Coudray[1,2,*], Georgia L. Isom[1,*], Mark R. MacRae[1,*], Mariyah N. Saiduddin[1], Gira Bhabha[1,‡], Damian C. Ekiert[1,3,‡]

[1] Department of Cell Biology, Skirball Institute of Biomolecular Medicine, New York University School of Medicine, New York, NY 10016, USA
[2] Applied Bioinformatics Laboratories, New York University School of Medicine, New York, NY, USA
[3] Department of Microbiology, New York University School of Medicine, New York, NY, USA
* These authors contributed equally to this work
‡ e-mail: damian.ekiert@ekiertlab.org; gira.bhabha@gmail.com

In double-membraned bacteria, phospholipids must be transported across the cell envelope to maintain the outer membrane barrier, which plays a key role in antibiotic resistance and pathogen virulence. The Mla pathway has been implicated in phospholipid trafficking and outer membrane integrity, but the mechanism by which this ABC transporter facilitates phospholipid transport remains unknown. Here we report the cryo-EM structure of the MlaFEDB inner membrane complex at 3.05 Å resolution. Our structure reveals that the core transporter subunit, MlaE, adopts an ABC exporter fold and is related to the lipopolysaccharide export system as well as the human lipid exporter families, ABCA and ABCG. Unexpectedly, two phospholipids are bound in the outward-facing pocket of MlaFEDB, raising the possibility that multiple lipid substrates may be translocated each transport cycle. The unusual configuration of bound lipids suggests that lipid reorientation may occur before extrusion through the hydrophobic MlaD pore. Site-specific crosslinking confirms that lipids bind in this pocket *in vivo*. Our structure supports a model in which the Mla system may drive phospholipid export to the bacterial outer membrane, and provides mechanistic insight into the function of an exporter family conserved from bacteria to humans.

ABC transporters are a structurally diverse group of membrane proteins that import and export a wide range of cargos across cellular membranes, powered by an ATP-binding cassette (ABC). ABC exporters have been implicated in the efflux of chemotherapeutics[1,2], antibiotics[3], lipids[4–7], and cholesterol[8]. Given their key roles in drug metabolism and disease in humans, as well as virulence in numerous bacterial pathogens, ABC exporters are the target of many drug development efforts. ABC exporters that facilitate lipid transport in double-membraned bacteria are critical in maintaining the integrity of the bacterial cell envelope, and present novel targets for antibiotic therapies. While structures of the LPS flippase[9–11] and the LPS export system[12–18] have recently been elucidated, and indeed have led to the development of novel inhibitors[19–21], comparatively little is known about mechanisms of bacterial phospholipid transport.

The Mla transport system plays an important role in phospholipid trafficking between the inner and outer membranes in Gram-negative bacteria and is important for maintaining the outer membrane barrier[22–34]. This pathway consists of three main parts: first, an inner membrane (IM) ABC transporter complex, MlaFEDB; second, an outer membrane (OM) complex, MlaA-OmpC/F, and third, a soluble periplasmic protein, MlaC, which has been proposed to shuttle phospholipids between MlaFEDB and MlaA-OmpC/F (**Fig. 1a**). The directionality of transport facilitated by the Mla pathway is still an area of intense research, with reports of both phospholipid import[22] and export[24,25]. The IM complex, MlaFEDB, consists of four different proteins: MlaD, a membrane anchored protein from the MCE (Mammalian Cell Entry) protein family, which forms a homohexameric ring in the periplasm[29,33]; MlaE (also called YrbE), a predicted integral inner membrane ABC permease; MlaF, an ABC ATPase; and MlaB, a STAS domain protein with possible regulatory function[35]. Crystal structures of MlaD[29] and MlaFB[35] have provided insights into the function of individual domains, and low resolution cryo electron microscopy (cryo-EM) structures[25,29] have established the overall shape of the complex. MlaE is the transmembrane subunit of MlaFEDB, and was previously hypothesized to have some similarity to the ABCA/ABCG/Lpt family of hydrophobic exporters[29], also known as the type II exporters[36,37]. However, MlaE is predicted to have fewer transmembrane helices and has minimal sequence similarity, making it unclear whether MlaE is a highly diverged member of the ABCA/ABCG/Lpt family or perhaps entirely unrelated. Thus, a structure of the MlaFEDB complex may provide

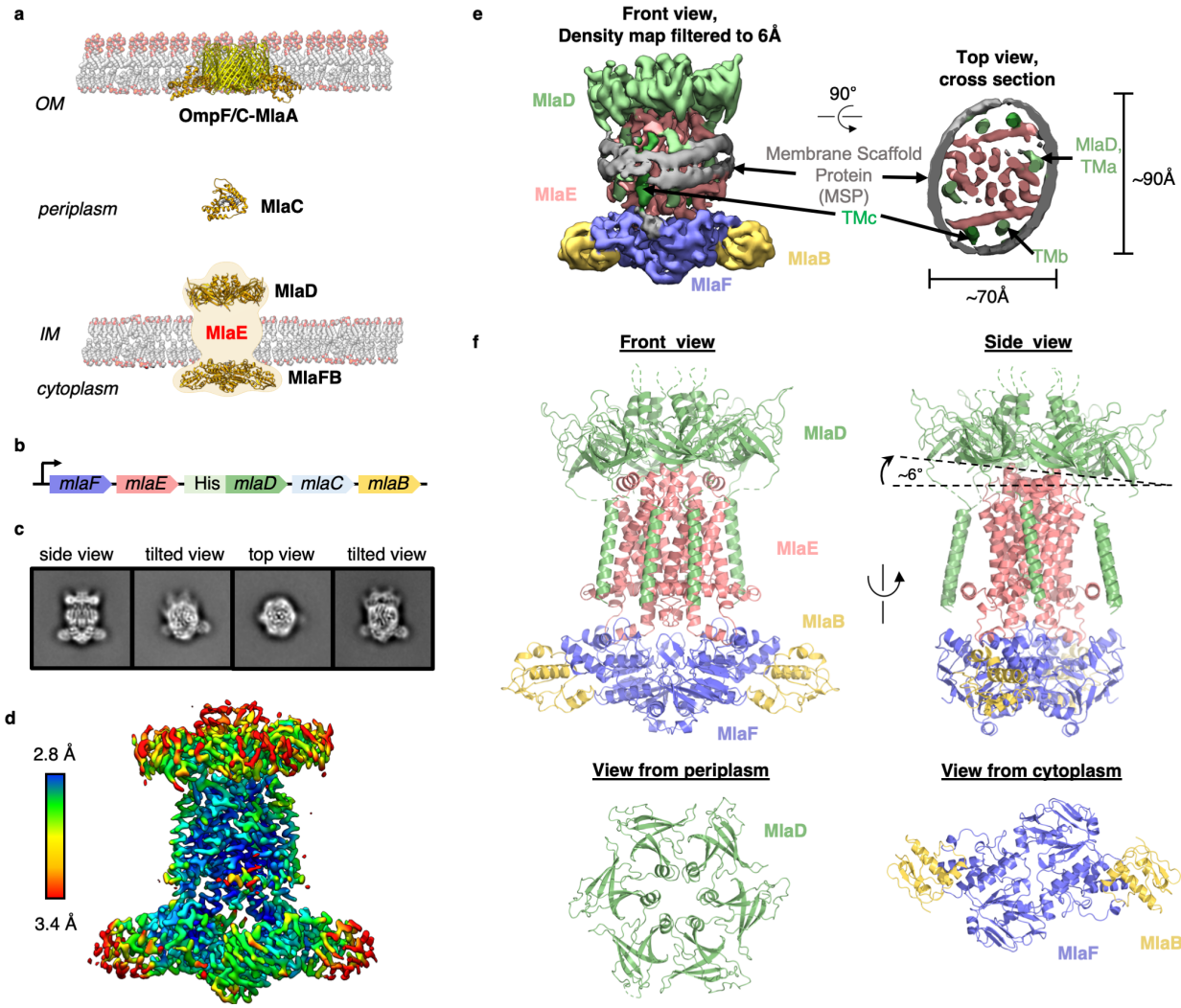

Figure 1. Cryo-EM structure of the MlaFEDB complex. (a) Schematic of the Mla pathway (adapted from[35]). The OmpF/C-Mla complex (PDB 5NUP), soluble protein MlaC (PDB 5UWA), and MlaFEDB complex (PDB 5UW2, EMDB-8610) are shown. **(b)** Schematic of the MlaFEDCB operon. **(c)** 2D class averages from single particle cryo-EM analysis of MlaFEDB in nanodiscs. **(d)** 3D reconstruction of MlaFEDB, colored by local resolution. **(e)** Density map of MlaFEDB filtered to 6 Å, showing membrane scaffold proteins (MSPs) of the nanodisc. MlaF, purple; MlaE, pink; MlaD, green; MlaB, yellow; MSP, grey. **(f)** Overview of the $MlaF_2E_2D_6B_2$ model; colors as in Fig. 1e.

important insights into the mechanisms of bacterial lipid transport, as well as the evolution and function of the broadly conserved type II exporter family.

Results

Overview of the MlaFEDB structure

To address how Mla drives lipid transport, we overexpressed the *mla* operon (**Fig. 1b**) and reconstituted the MlaFEDB complex in lipid nanodiscs, in the presence of *E. coli* polar lipids (see Methods), and determined a 3.05 Å structure using single particle cryo-EM (**Supplementary Table S1**, **Fig. S1, Fig. 1c-e)**. Although MlaFEDB was expected to exhibit 2-fold symmetry, initial reconstructions showed clear asymmetry in our maps, which we then refined to high resolution without applying symmetry (**Fig. 1d, Fig. S1, Supplementary Table S2**). Local resolution analysis showed that the entire complex is well-defined at ~2.8 - 3.5 Å resolution (**Fig. 1d, Fig. S2a**), allowing us to build a nearly complete model for MlaFEDB (**Fig. 1f**), including a high-resolution structure of the MlaE subunit. In addition, we resolved both coils of the membrane scaffold protein (MSP) belt surrounding the nanodisc[38] (**Fig. 1e, Fig. S2b**).

The MlaFEDB transporter is significantly larger and more complicated than most ABC transporter structures determined to date. The complex consists of a total of 12 polypeptide chains from 4 different genes, with a stoichiometry of $MlaF_2E_2D_6B_2$. At the center of the complex, a core ABC transporter module is formed from two copies each of the MlaF ATPase and the MlaE transmembrane domains (TMDs). Outside this ABC

transporter core, MlaFEDB contains additional subunits not found in other ABC transporters: MlaD on the periplasmic side of the IM, and MlaB in the cytoplasm. A homohexameric ring of MCE domains from MlaD sits atop the periplasmic end of MlaE like a crown. This MCE ring is anchored in place by six MlaD transmembrane helices, which dock around the periphery of the MlaE TMDs (**Fig. 1f**). On the cytoplasmic side, each of the MlaF ATPase subunits is bound to MlaB, a STAS (Sulfate Transporter and Anti-Sigma factor antagonist) domain protein that was recently reported to act as regulator of the MlaFEDB transporter[35]. The overall structure of the $MlaF_2B_2$ module is very similar to our recent MlaFB X-ray structure, apart from a small relative rotation between the MlaF helical and catalytic subdomains (**Fig. S3a**). This rotation is similar to motions described in other ABC transporters[39–41]. An unusual C-terminal extension of each MlaF protomer wraps around the neighboring MlaF subunit and docks near the MlaFB interface, almost identical to the domain-swapped "handshake" motif observed in the crystal structure of the $MlaF_2B_2$ subcomplex (**Fig. S3b**). While the MlaFEB subcomplex exhibits near-perfect 2-fold rotational symmetry, the MlaD ring is tilted relative to MlaE, resulting in a misalignment of the 2-fold symmetry axis of MlaFEB and the pseudo-6-fold axis of MlaD by approximately 6 degrees (**Fig. 1f**).

MlaE adopts an exporter fold

The transmembrane subunits of ABC transporters play a central role in determining the specificity of substrates and the direction of substrate translocation. Consequently, the structure of the MlaE subunit is of particular interest. Our cryo-EM structure reveals that the core TMD of MlaE consists of 5 transmembrane helices (TM1 - TM5) (**Fig. 2a, 2b**). Two additional N-terminal helices are membrane embedded, which we call interfacial helices 1 and 2 (IF1 and IF2[42]; discussed in more detail below). A coupling helix (CH) in the cytoplasm connects TM2 and TM3, and mediates the interaction between the TMDs of MlaE and the MlaF ATPase subunits (**Fig. S3c**), similar to other ABC transporters[43,44]. Lastly, a small periplasmic helix

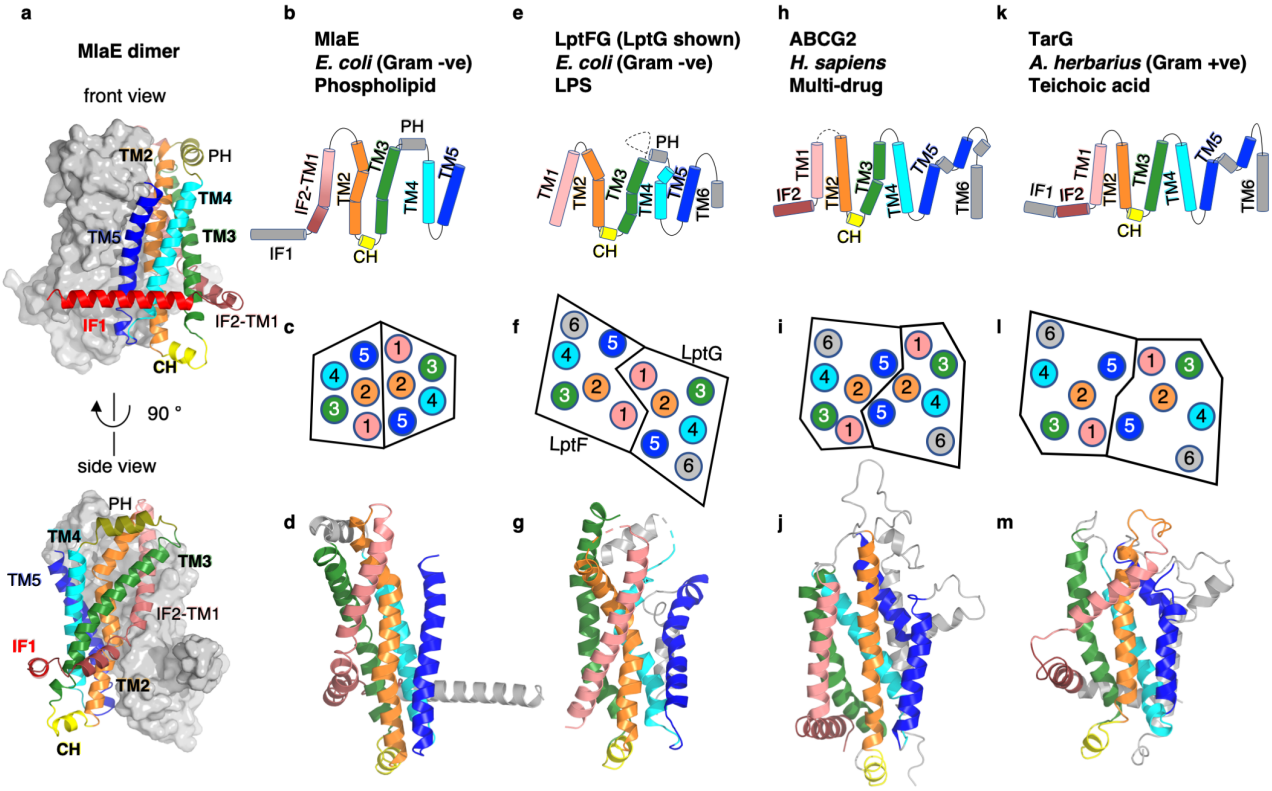

Figure 2. The fold of MlaE resembles type II ABC exporters. (a) MlaE dimer, with one dimer represented as surface, and the other as cartoon. **(b-m)** comparisons of the transmembrane domains of type II exporters including: MlaE, LptG (PDB 6MHZ), ABCG2 (PDB 6HBU) and TarG (PDB 6JBH). **(b, e, h, k)** Topology diagrams. **(c, f, i, l)** Schematics representing helices at the dimer interface, viewed from the cytoplasm (each circle represents a helix). **(d, g, j, m)** Cartoon view of monomer, see **Fig. S4a** for more examples. CH, coupling helix; PH, periplasmic helix; IF, interfacial helix (also called connecting helix in ABCG transporters); TM, transmembrane helix.

(PH) is found between TM3 and TM4 at the periplasmic side of MlaE.

Strikingly, the MlaE fold is homologous to a diverse family of transporters called the "type II exporters" (**Fig. 2b-m, Fig. S4a**)[36,37]. Type II exporters like MlaE are broadly distributed in both eukaryotes and prokaryotes and include several important lipid exporters found in both Gram-positive and Gram-negative bacteria, such as: 1) the LPS exporter, LptFG[12,14,43,45,46] (**Fig. 2e**); 2) the O-antigen exporter, Wzm[44,47] (**Fig S4a**); and 3) the teichoic acid exporter, TarG[42] (**Fig. 2k**). Also within this family are the human exporter subgroups ABCA and ABCG, which are clear homologs of MlaE, and include 4) the phospholipid exporter, ABCA1[48] (**Fig. S4a)**; 5) the cholesterol exporter, ABCG5/G8[36] (**Fig. S4a**); and 6) the hydrophobic multi-drug resistance (MDR) efflux pump, ABCG2[2,49,50] (**Fig. 2h**). As all of these type II exporters are known to drive hydrophobic transport, share a well-conserved fold, and likely evolved from a common protein ancestor, placement of MlaE in this family provides strong structural evidence that MlaFEDB likely functions as a phospholipid exporter. While we favor this exporter model for MlaFEDB, we cannot rule out the possibility that MlaE instead functions in lipid import; in that scenario, MlaE would represent the first example of an ABC transporter with a type II exporter fold that in fact functions as an importer.

While the core fold of the TMD is conserved among members of the type II exporter family, other regions are more variable. First, MlaE is missing a 6th transmembrane helix (TM6) which is present near the periphery in all other structurally characterized members of the family (**Fig. 2b-m, Fig. S4a**). Thus, TM1-TM5 of MlaE define the minimal core domain of the type II exporter fold that is shared among all family members. Second, in both MlaE and LptFG, TM5 exists as one continuous helix, whereas the structures of other family members have a small insertion near the periplasmic end that results in a pair of reentrant helices (**Fig. S4b**). Third, most type II exporters have a membrane-embedded helix preceding TM1, which we call IF2 (also called CnH[36] and IF[44]). Together, IF2 and TM1 adopt a continuum of states across this transporter family. At one extreme, IF2 forms an amphipathic helix that runs roughly parallel to the membrane within the cytoplasmic leaflet, followed by a turn and a separate TM1, which spans nearly the entire bilayer (**Fig. S4c;** teichoic acid transporter). At the other extreme, it appears that IF2 and TM1 may be fused to form a long, continuous helix (**Fig. S4c;** in LptF and LptG). In MlaE, this region adopts an intermediate configuration, where IF2 and TM1 are both involved in the first traverse of the membrane, but these two segments are distinguished by a clear kink in the middle of the membrane (**Fig. S4c**). Overall, the structure of the transmembrane region of MlaE most closely resembles the LptFG subunits from the LPS exporter, perhaps reflecting similar functions in membrane lipid extraction and export towards the outer membrane.

MlaE IF1 helix creates a unique membrane environment

Outside the core TMD, the region surrounding the MlaFEDB complex is unusually loose and open to membrane lipids. This unique environment is created by the IF1 helix of MlaE and the 6 TM helices from MlaD. The IF1 helix is a 30 residue long, amphipathic N-terminal helix that lies parallel to the membrane within the cytoplasmic leaflet, and extends along the width of the MlaE dimer (**Fig. 2a**). We denote this helix as IF1 as it precedes IF2, and is reminiscent of IF1 in TarG[42], but lies in a structurally distinct location. While the C-terminal portion of IF1 interacts with TM3 and TM4, the N-terminal half projects outward into the surrounding membrane, creating a cleft between the core TMD and the IF1 helix (**Fig. 3a**). Second, the 6 TM helices from MlaD, one from each subunit, bind around the outside of the central MlaE dimer and anchor the MCE ring to the membrane (**Fig. 3a**). Due to the symmetry mismatch between the pseudo-6-fold symmetric MlaD ring and the 2-fold symmetric MlaFEB module, the identical transmembrane helices of MlaD interact with MlaE in 3 non-equivalent ways. Distinct interactions are mediated by MlaD chains A+D (MlaD-TM$^{A/D}$), MlaD chains B+E (MlaD-TM$^{B/E}$) and MlaD chains C+F (MlaD-TM$^{C/F}$) (**Fig. 3a**). Four of the TM helices, MlaD-TM$^{B/E}$ and MlaD-TM$^{C/F}$, are largely isolated in the membrane, and their main interactions are with the MlaE IF1 helices in a ~84 degree helix crossing interaction, which is relatively rare in transmembrane proteins. Since larger side chains would clash and destabilize the interaction, this helical packing geometry enforces a strong preference for glycine residues at the positions of closest contact: between IF1 and MlaD-TM$^{B/E}$ (Gly21^{MlaE} and Gly11^{MlaD}, ~3.4 Å Cα-Cα); and between IF1 and MlaD-TM$^{C/F}$ (Gly10^{MlaE} and Gly11^{MlaD}, ~3.5 Å Cα-Cα) (**Fig. S5a**). Gly is present at MlaD position 11 in 13/13 sequences analyzed, and at MlaE positions 10 and 21 in 12/13 sequences analyzed (**Fig. S5c, and Methods**), suggesting that the interactions between IF1, MlaD-TM$^{B/E}$, and MlaD-TM$^{C/F}$ are specific and conserved. Compared to these relatively sparse helix crossing interactions, the remaining 2 TM helices, MlaD-TM$^{A/D}$, interact more intimately with the outside of the MlaE TMD core, making contact with IF2, TM1, TM3, and the short periplasmic helix (**Fig. S5b**).

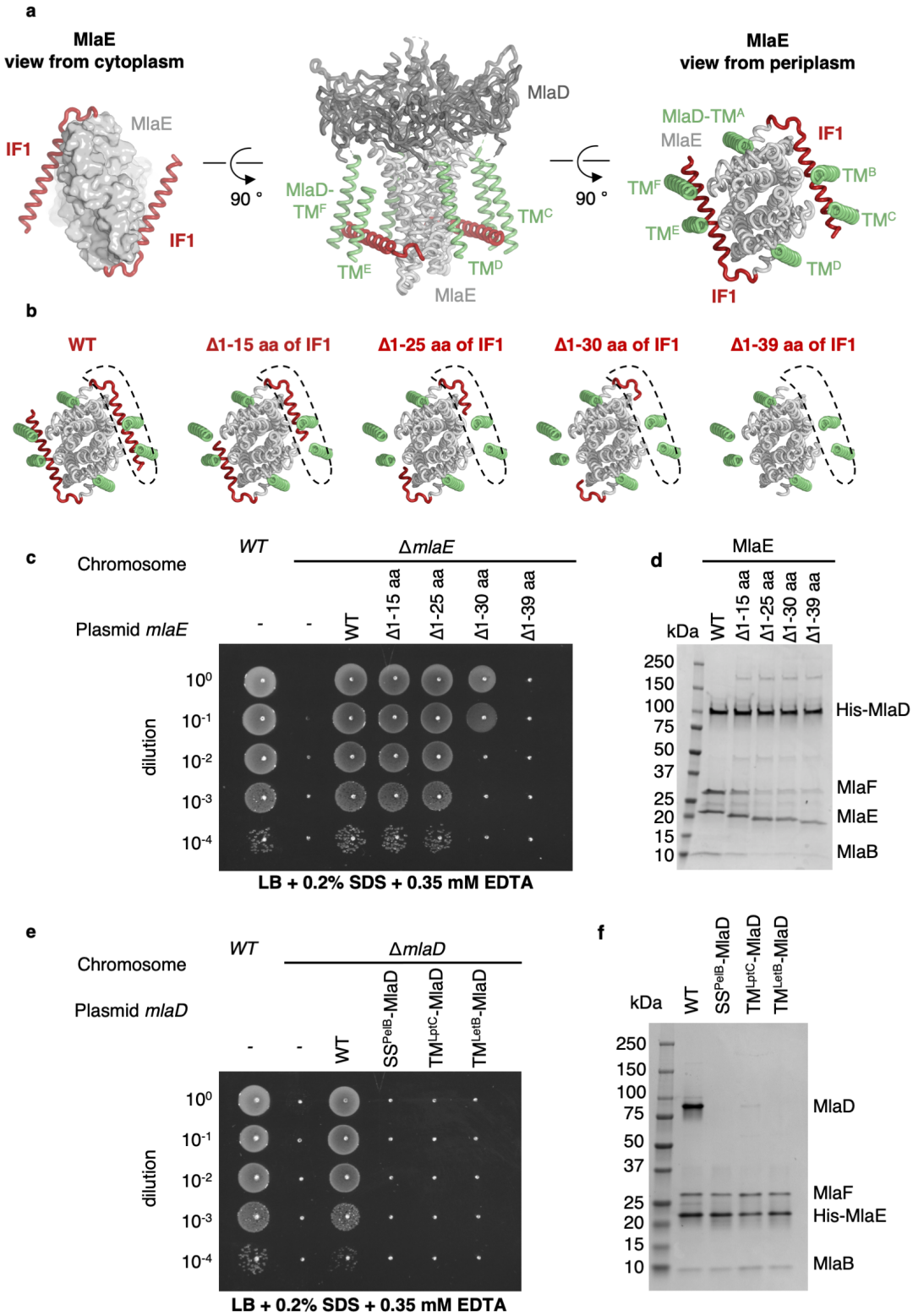

Figure 3. The role of the MlaE IF1 helix and the MlaD the transmembrane helices in cellular assays. (a) Bottom, side and top views highlighting IF1 (red), its orientation in the MlaFEDB complex, and its interaction with the six transmembrane helices of MlaD (annotated TMa to TMf). **(b)** Illustration of the IF1 truncation mutants used in genetic complementation assays. **(c, e)** Cellular assay for the function of MlaE and MlaD**.** 10-fold serial dilutions of the indicated cultures spotted LB plates containing SDS and EDTA at the concentrations indicated (bottom) and incubated overnight. The *mlaE* and *mlaD* single knockouts grow poorly in the presence of SDS+EDTA, but can be rescued by the expression of WT MlaE or MlaD constructs, respectively. Shorter MlaE IF1 truncations fail to restore growth of an *mlaE* knockout strain, while mutants retaining longer versions of MlaE IF1 fully rescue the knockout strain **(c)**. All MlaD transmembrane helix mutants fail to complement the *MlaD* knockout strain **(e)**. Corresponding controls plated on LB only can be found in **Fig. S5d and S6b**. **(d,f)** SDS PAGE of recombinantly expressed and purified protein resulting from mutants in (**c)** and (**e**). Protein was purified by affinity chromatography, using the affinity-tagged protein as indicated on the figure.

IF1 represents a highly unusual feature of the MlaFEDB transmembrane region. To assess its role in the function of the transporter, we generated a series of truncation mutants of MlaE IF1, and tested their ability to complement an *mlaE* knockout strain of *E. coli*. Mutations in components of the Mla pathway exhibit a substantial growth defect in LB medium in the presence of SDS+EDTA[22], which can be complemented with WT *mlaFEDCB* on a plasmid (**Fig. 3c, S5d**). MlaE mutants with 15 or 25 residues deleted from the N-terminus of IF1 (Δ1-15 aa and Δ1-25 aa) fully restored growth of an *mlaE* knockout in this assay, similar to complementation by the WT operon, despite the fact that this deletion removes the binding sites for 4 out of 6 MlaD TM helices (**Fig. 3b-c**). However, MlaE mutants with larger deletions only partially restored growth (Δ1-30 aa), or failed to complement (Δ1-39 aa). To assess whether the IF truncation mutants exhibit defects in protein expression or complex formation, we overexpressed and purified each of the mutant MlaFEDB complexes with a His-tag on MlaD. SDS-PAGE revealed that all the MlaE mutants expressed well, and bind to MlaD (**Fig. 3d**). However, truncations of IF1 led to reduced incorporation of MlaF and MlaB into the MlaFEDB complex following affinity purification. Thus IF1 appears to be important for the integrity and stability of the MlaFEDB complex.

MlaD TM helices are required for MlaFEDB assembly

MlaD has two main modes of interaction with MlaE: First, the 6 TM helices of MlaD interact with MlaE within the transmembrane region; second, the membrane-proximal surface of the MlaD ring contributes a large interaction interface with the periplasm-facing surface of MlaE (**Fig. S6a**). To address the functional importance of the MlaD TM helix interactions, we generated variants of MlaD in which we replaced the TM helix with a TM helix expected to make no direct interactions with MlaE [from the *E. coli* IM proteins LptC (TM^{LptC}) or LetB (TM^{LetB})]. In addition, we tested a soluble, periplasmic form of the MlaD ring, in which the TM helix was replaced by the PelB secretion sequence (SS^{PelB}). We used the same complementation assay described above to assess the function of these variants in cells. We found that none of the MlaD TM variants were able to restore growth of an *mlaD* knockout strain in the presence of SDS+EDTA (**Fig. 3e, S6b**). To assess whether these MlaD variants are still capable of interacting to form MlaFEDB complexes, we recombinantly overexpressed each of these variants in the context of the *mla* operon, and purified the resulting complexes using an affinity tag on MlaE. SDS-PAGE showed that MlaE co-purified with MlaB, MlaF and WT MlaD, but mutant forms of MlaD did not co-purify (**Fig. 3f**), despite robust expression levels of hexameric MlaD detected in the membrane fraction (TM^{LptC}-MlaD / TM^{LetB}-MlaD chimeras), implying that these two proteins are well-folded and properly localized (**Fig. S6c**). Thus, the mere presence of MlaD hexamers anchored to the membrane is not sufficient to complement an *mlaD* knock-out, but rather MlaD appears to require its native TM helix in order to assemble and function in complex with MlaFEDB. These results suggest that the MlaD TM helix interactions with MlaE drive specificity in the formation of the complex.

MlaE adopts an outward-open conformation in the apo state

While the vast majority of ABC transporter structures adopt an inward-open conformation in the absence of nucleotide[50–53], our structure of MlaE is in the outward-open state (**Fig. 4a**). The ATP-binding sites in the MlaF dimer are clearly empty (without any density visible in the binding pockets), confirming that our MlaFB structure is in the apo state. This uncommon configuration was previously observed in the closely related type II exporter LptFG[14,54], suggesting that the ATP driven transport of phospholipids and LPS may share many mechanistic features. The TMD of the structurally unrelated MacAB-TolC efflux pump is also outward-open in the apo state[3]. The narrow outward-open pocket within MlaE encloses a volume of ~750 $Å^3$ (estimated using CASTp[55]), and is primarily formed by TM1 and TM2, with some contribution from TM5 (**Fig. 4a**). This is similar to LptFG, where TM1, TM2, and TM5 form a much larger pocket (volume of ~3000 $Å^3$, estimated using CASTp[55], in PDB: 6MHU[12]) at the periplasmic side of the complex for LPS binding. The pockets in both transporters are largely hydrophobic in nature, consistent with binding to lipid substrates, though in LptFG the rim has a pronounced positive charge proposed to interact with phosphates on the LPS inner core[12], while MlaE is more neutral.

MlaD forms a hexameric MCE ring with a hydrophobic pore at the center[29]. Similar hydrophobic tunnels have been observed through the MCE rings of PqiB and LetB[29,56], and phospholipids have been crosslinked inside the tunnel of LetB. Indeed, in our structure of the MlaFEDB complex, the pore of MlaD and the outward-facing pocket of MlaE align, resulting in a continuous hydrophobic tunnel that runs from the pocket of MlaE, through MlaD, and out into the periplasm (**Fig. 4b**). Large and structurally diverse lipid transport domains are an integral part of many members of the type II exporter family[12,14,48] (**Fig. S7a**), perhaps in light of the challenges associated with effluxing hydrophobic molecules through the aqueous extracellular/periplasmic environment.

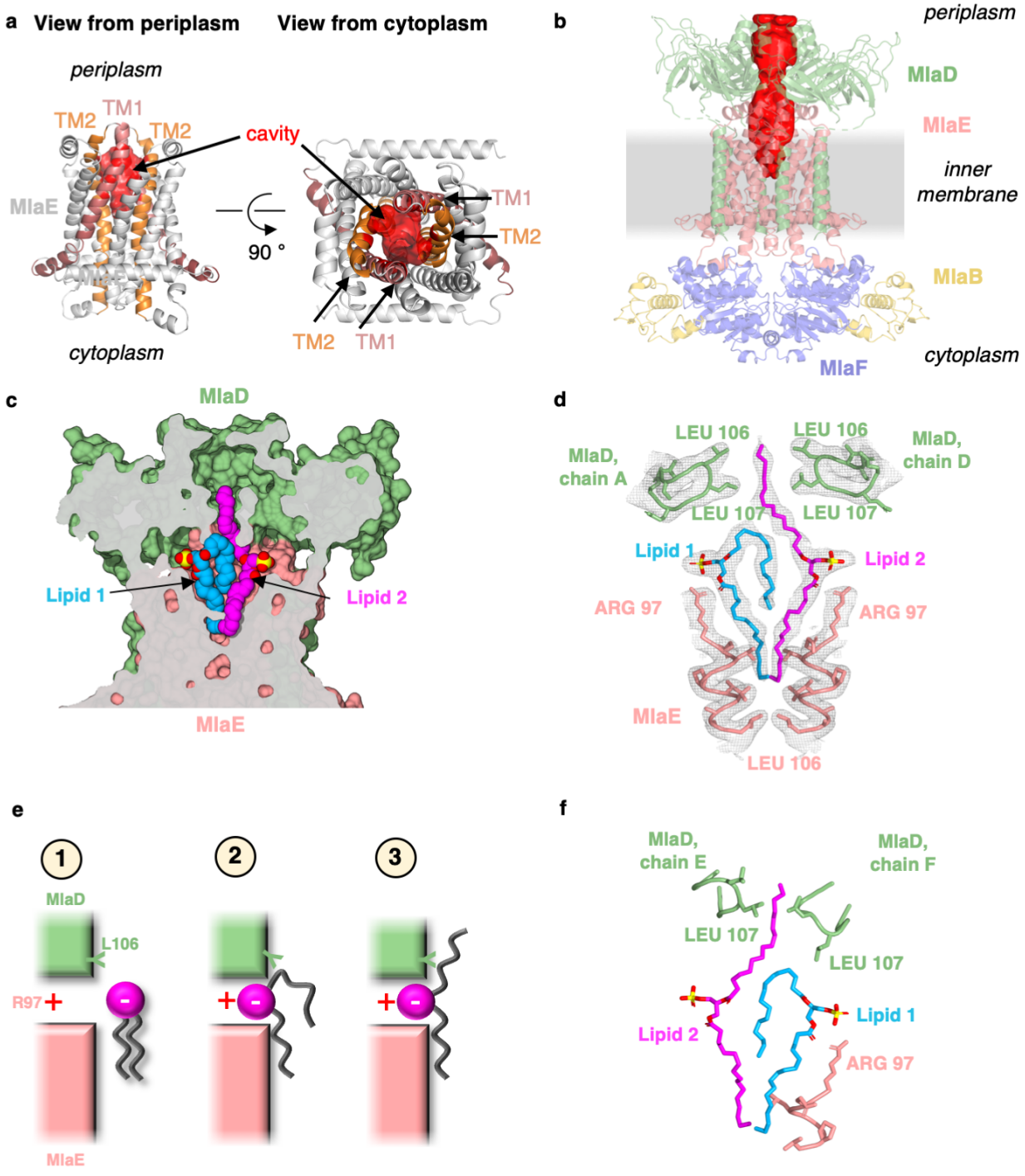

Figure 4. Two lipids are bound in the lipid binding pocket formed by MlaE and MlaD. (a) MlaE adopts an outward-open conformation in the absence of nucleotide. The boundary of the substrate binding pocket was estimated using CASTp[55], and is displayed as a red surface. Viewed from the side with the cytoplasm down and periplasm up (left), and viewed from the top, looking down from the periplasm (right). **(b)** A continuous hydrophobic tunnel runs from the substrate binding pocket in MlaE through MlaD's pore to the periplasmic space (red, tunnel boundary estimated with HOLLOW[77]). **(c)** Side view cross-section of the lipid translocation pathway between MlaE and MlaD showing the two bound phospholipids, shown in blue and magenta. **(d)** Zoom in view of the lipids and surrounding structural elements and key residues. EM density map is shown as mesh, highlighting the unambiguous lipid densities and adjacent protein sidechains. **(e)** Model for potential strain-induced lipid flipping mechanism. Interactions between Arg97 and phosphate head groups may promote lipid inversion. **(f)** Asymmetric interactions between MlaE and MlaD are mediated indirectly by phospholipid substrates via an interaction with Leu107 and the fatty acid tails.

Two lipids are bound in the substrate-translocation pathway

Unexpectedly, two clearly defined diacyl phospholipids are bound in the outward-facing pocket of MlaE (**Fig. 4c and S8a**), suggesting that the Mla system may transport two substrates per ATP cycle. Structures of the periplasmic lipid carrier protein, MlaC, have been determined with either 1 or 2 phospholipids bound[29] **(Fig. S7b**), and a structure of apo *E. coli* MlaC revealed a "clamshell'-like motion resulting in significant changes in the volume of the lipid binding pocket[24]. The different architectures and conformational states of the MlaC pocket suggest that it may accommodate one or two phospholipids, or larger substrate molecules. Indeed, previous studies have suggested that cardiolipin may be a substrate of the Mla system[25], and that cardiolipin is detected by TLC on lipid extracts from components of the Mla system[24]. Together with previous functional data, the presence of 2 phospholipids/4 acyl chains bound in our MlaFEDB structure raises the possibility that the Mla system may be capable of transporting tetra-acyl lipids, such as cardiolipin.

Unlike recent structures of the LPS exporter bound to LPS, where all of the acyl chains project downward into the hydrophobic pocket of LptFG[45,54], the lipids bound to MlaFEDB appear to be trapped in the process of being extruded and transferred to the MlaD pore. In one lipid molecule (lipid 1), both acyl chains are bound in the pocket of MlaE (**Fig. 4d**). Strikingly, the second lipid (lipid 2) adopts an extended conformation, with one acyl chain reaching down into the MlaE pocket while the other projects upwards to insert into a constriction in the MlaD pore. The pore is formed by Leu106 and Leu107 residues from each of the 6 subunits in the MlaD ring (**Fig 4d-e**), which have previously been implicated in MlaD function[29]. In contrast to the hydrophobic fatty acid tails, which are completely buried within the MlaE-MlaD tunnel, the polar head group of each lipid projects outwards through lateral solvent accessible channels on opposite sides of the complex, where Arg97 from each MlaE subunit forms a salt bridge with the phosphate head group (**Fig. 4d**). Binding of the head group in the lateral channels seems likely to induce strain and asymmetry in the glycerol backbone and aliphatic regions that may help to initiate reorientation (**Fig. 4e)**. This distortion from bilayer geometry is observed in lipid 1 where the uppermost acyl chain arcs upwards before turning back down into the pocket of MlaE (**Fig. 4d**). Thus, lipid 1 may represent an initial distorted state that transitions to the extended conformation of lipid 2, potentially the halfway-point in the process of completely inverting the orientation of the lipid: from "tails-down" as if embedded in the outer leaflet of the membrane, to "tails-up" as it traverses the MlaD pore. Reorienting the lipids may be important to ensure that they emerge into the periplasm from the MlaD pore tails-first, to facilitate their binding to MlaC, which recognizes only the tails[29]. However, it

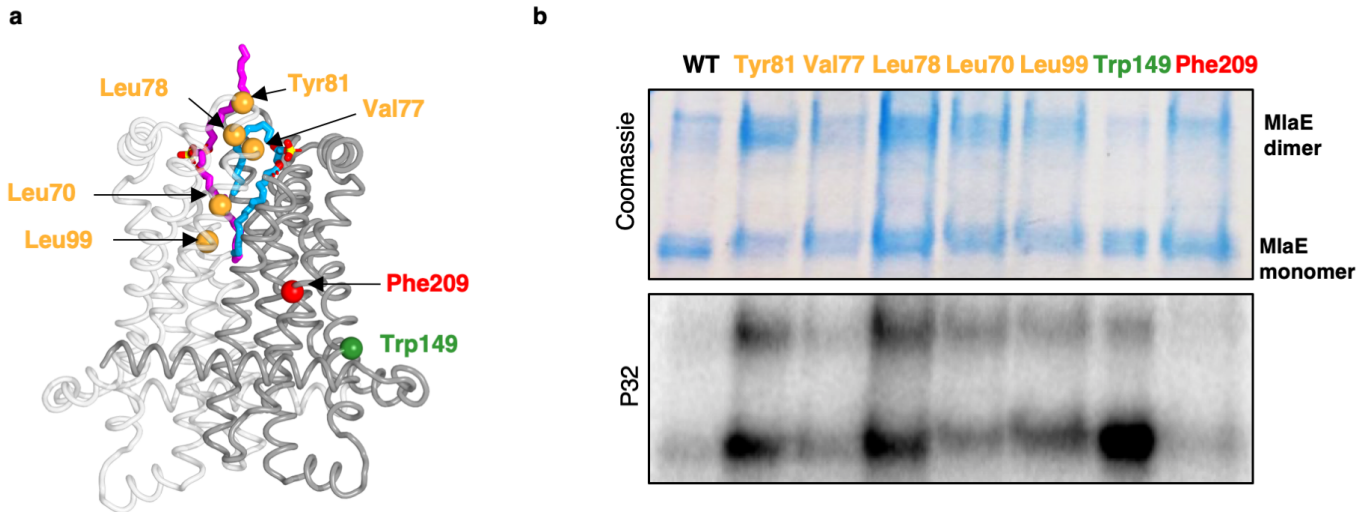

Figure 5. ***In vivo*** **photocrosslinking of lipids bound to MlaFEDB. (a)** Residues in MlaE for which individual mutants were generated and tested in photocrosslinking experiments are shown as spheres in the context of the MlaE dimer (cartoon). orange, residues in the lipid-binding pocket; red, residue buried within MlaE, designed as a negative control; green, residue facing the membrane environment, designed as a positive control. The two lipids are shown in magenta and blue sticks. **(b)** SDS-PAGE analysis of purified MlaFEDB and BPA mutants, stained by Coomassie (protein) or phosphor-images (^{32}P signal). We observed MlaE in both its monomeric and dimeric state, as confirmed by Western blot (**Fig. S9**), the latter of which was enriched in some of the mutants, likely due to formation of crosslinks between the two MlaE monomers.

is also possible that lipids move through the pore in an extended state, perhaps allowing MlaC to first bind to one tail, followed by the second.

Viewed from the side, the MlaD ring is tilted with respect to MlaFEB by approximately 6 degrees, and deviates from the expected 6-fold symmetry observed in the crystal structure of MlaD and other MCE proteins, including re-organization of 2 of the 6 pore lining loops as well as domain level rearrangements in the ring (**Fig. S8b-c**). This is particularly surprising, as the MlaFEB module of our EM structure is 2-fold symmetric and the crystal structure of the MlaD ring in isolation exhibited near perfect 6-fold symmetry. This raises the question: what is breaking the symmetry in our MlaFEDB structure? The clear density for the two bound phospholipids suggests that the asymmetry of the MlaD ring and the configuration of the lipids is tightly correlated. Thus, the asymmetry in MlaD seems to arise from its asymmetric interactions with lipid 1 at the interface of MlaE and MlaD. Leu107 from MlaD chain F makes hydrophobic interactions with one of the fatty acid tails, perhaps stabilizing this side of the MlaD ring in closer proximity to MlaE and the lipid binding pocket (**Fig. 4f**). Thus, we propose that MlaD is sensitive to the configuration of lipids in the pocket of MlaE, and these conformational changes in the MlaD ring may be important for lipid translocation through the channel or perhaps even modulating the binding of MlaC to the transporter.

To assess whether phospholipids are bound in the pocket of MlaE in cells, we utilized a site-specific photocrosslinking method[56] to detect binding of radiolabeled phospholipids *in vivo*. We incorporated the unnatural photocrosslinking amino acid *p*-benzoyl-L-phenylalanine (BPA)[57] into the MlaE protein at five positions in the lipid binding site (Leu70, Val77, Leu78, Tyr81, and Leu99), as well as Phe209 (protected in the MlaE core; not expected to bind lipids) or Trp149 (membrane exposed; expected to non-specifically bind lipids) (**Fig. 5a**). After crosslinking in cells grown in the presence of ^{32}P orthophosphate to label total phospholipids, these MlaE proteins were purified and analyzed by SDS-PAGE. crosslinking at Trp149 and Phe209 resulted in high and low ^{32}P signal, respectively, indicative of an abundance of phospholipids near the membrane-exposed Trp149 and very few phospholipids near the buried Phe209, as expected (**Fig. 5b**). ^{32}P incorporation into MlaE was induced by a crosslinkers positioned in the outward-facing lipid binding pocket, most prominently at Tyr81 and Leu78, to a lesser extent at Leu70 and Leu99, and weakly at Val77. Thus, the phospholipid binding site observed in our MlaFEDB structure is occupied by phospholipids *in vivo*.

Discussion

Together, the results presented here lead to our current understanding of lipid transport by the Mla system, and provide evidence that the system likely functions as an exporter. A role for MlaFEDB in phospholipid export is also supported by recent cellular studies in *Acinetobacter baumannii*[25], as well as *in vitro* experiments with *E. coli* proteins, showing lipid directional transfer from MlaD to MlaC[24,26]. Although we do not rule out the possibility that Mla may drive retrograde transport, as reported in other studies[22,27,32,34] we favor a model for anterograde phospholipid export by Mla in light of the structural similarities between MlaE and other type II ABC exporters (**Fig. 6**). In our model for Mla-mediated lipid export, first, phospholipids must be extracted from the inner membrane and reach the outward-facing pocket of MlaE, from either the inner or outer leaflet. Due to the structural similarities between MlaE and LptFG, which extracts LPS from the outer leaflet, it is plausible that MlaFEDB may extract PLs from the outer leaflet as well, particularly as other proteins have been implicated in PL flipping between leaflets, such as MsbA[58,59]. However, as some other

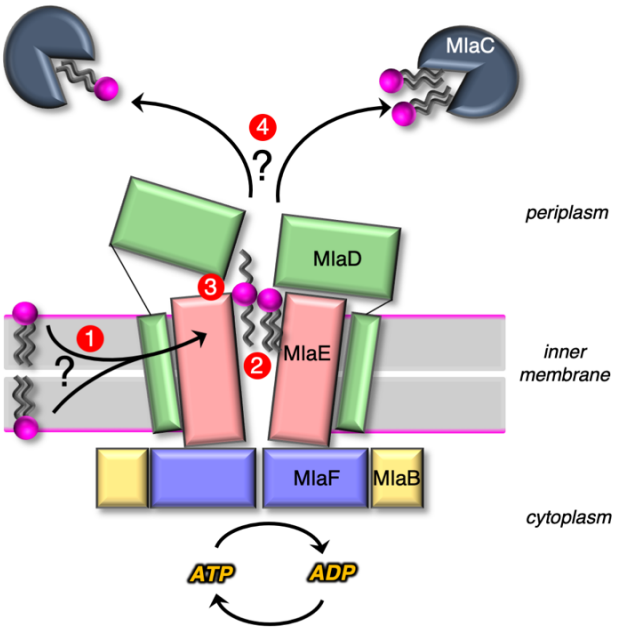

Figure 6. Model for lipid transport export by MlaFEDB. 1) Lipids are extracted from the IM and transferred to the outward facing pocket by an unknown mechanism. 2) Lipids are reoriented, from “tails-down” to “extended” or “tails-up” configuration, perhaps aided by strain induced by head group binding. 3) Conformational changes in MlaE coupled to the ATP hydrolysis cycle push lipids out of MlaE pocket and into MlaD pore. 4) Lipids are transferred to MlaC to be shuttled across periplasm to the outer membrane MlaA-OmpC/F complex.

type II exporters are known to flip lipids from the inner to outer leaflet[42,44], it is also possible that MlaFEDB may flip lipids across the bilayer before exporting them. Second, reorientation of the lipids may occur such that they move through the MlaD pore "tails-first", or perhaps in an extended conformation, to facilitate transfer from MlaD to MlaC. The process may be assisted by the energy of head group binding to the lateral channels and distortion of the lipid away from "bilayer" geometry. Third, by analogy to the LPS exporter and other ABC transporters[12,14,48], we hypothesize that conformational changes in MlaE lead to a collapse of the outward-facing pocket, extruding the lipids upwards and into the pore through MlaD. In the LPS exporter, this step is thought to be linked to ATP binding or hydrolysis, and it is possible that lipid reorientation and pocket collapse occur in a concerted manner, as opposed to sequentially. In the fourth and final step of our model, the phospholipid emerges from the MlaD pore "tails-first" and is transferred to the lipid binding pocket of an MlaC protein docked on the surface of MlaD. As MlaC proteins from some species are capable of binding multiple phospholipids at one time[29], it is possible that two lipids may be transferred from MlaFEDB to a single MlaC protein. To complete the transport process, MlaC would then shuttle phospholipids across the periplasmic space and deliver them to the MlaA-OmpF/C complex for insertion into the outer membrane. Together, our data suggest a possible mechanism for phospholipid export across the cell envelope, and raise the intriguing possibility that Mla may translocate multiple phospholipid substrates each transport cycle, or perhaps accommodate larger lipid substrates like cardiolipin. A defined lipid binding pocket within MlaE sets the stage for future studies of targeted inhibitors and small molecule modulators of this complex, both in the context of therapeutics against drug-resistant Gram-negative bacteria, and for the study of cell envelope biogenesis in double-membraned bacteria.

Methods

Expression and purification of MlaFEDB

To prepare a sample for cryo-EM, plasmid pBEL1200[29], which contains the *mlaFEDCB* operon with an N-terminal his-tag on MlaD, was transformed into Rosetta 2 (DE3) cells (Novagen). For expression, overnight cultures of Rosetta 2 (DE3)/pBEL1200 were diluted 1:100 in LB (Difco) supplemented with carbenicillin (100 µg/mL) and chloramphenicol (38 µg/mL) and grown at 37 °C with shaking to an OD600 of 0.9, then induced by addition of L-arabinose to a final concentration of 0.2% and continued incubation for 4 hours shaking at 37 °C. Cultures were harvested by centrifugation, and the pellets were resuspended in lysis buffer (50 mM Tris pH 8.0, 300 mM NaCl, 10% glycerol). Cells were lysed by two passes through an Emulsiflex-C3 cell disruptor (Avestin), then centrifuged at 15,000 xg for 30 mins to pellet cell debris. The clarified lysates were ultracentrifuged at 37, 000 rpm (F37L Fixed-Angle Rotor, Thermo-Fisher) for 45 mins to isolate membranes. The membranes were resuspended in membrane solubilization buffer (50 mM Tris pH 8.0, 300 mM NaCl, 10% glycerol, 25 mM DDM) and incubated for 1 hour, rocking at 4 °C. The solubilized membranes were then ultracentrifuged again at 180,000 xg for 45 mins, to pellet any insoluble material. The supernatant was incubated with NiNTA resin (Fisher Scientific, #45-002-985) at 4 °C, which was subsequently washed with Ni Wash Buffer (50 mM Tris pH 8.0, 300 mM NaCl, 10 mM imidazole, 10% glycerol, 0.5 mM DDM) and bound proteins eluted with Ni Elution Buffer (50 mM Tris pH 8.0, 300 mM NaCl, 250 mM imidazole, 10% glycerol, 0.5 mM DDM). MlaFEDB containing fractions eluted from the NiNTA column were pooled and concentrated before separation on a Superdex 200 16/60 gel filtration column (GE Healthcare) equilibrated in gel filtration buffer (20 mM Tris pH 8.0, 150 mM NaCl, 10% glycerol, 0.5 mM DDM).

For all other MlaFEDB purifications mentioned in the manuscript, the sample was prepared in the same manner, but without size exclusion chromatography.

Reconstitution of MlaFEDB in lipid nanodiscs

The nanodiscs consisted of 3 components: MlaFEDB (expressed from pBEL1200 as described above), the membrane scaffold protein MSP1D1 and *E. coli* polar lipid extract (Avanti #100600).

For expression of the membrane scaffold protein, MSP1D1, overnight cultures of Rosetta 2 (DE3)/pMSP1D1 were diluted 1:100 in LB (Difco, #244620) supplemented with kanamycin (50 µg/mL) and chloramphenicol (38 µg/mL) and grown at 37 °C with shaking to an OD600 of 0.9, then induced by addition of IPTG to a final concentration of 1 mM and continued incubation for 3 hours shaking at 37 °C. Cultures were harvested by centrifugation, and the pellets were resuspended in lysis buffer (50 mM Tris pH 8.0, 300 mM NaCl, 10 mM imidazole). Cells were lysed by two passes through an Emulsiflex-C3 cell disruptor (Avestin), then centrifuged at 38,000 xg to pellet cell debris. The clarified lysates were incubated with NiNTA resin (Fisher Scientific, #45-002-985) at 4 °C, which was subsequently washed with Ni Wash Buffer (50 mM Tris pH 8.0, 300 mM NaCl, 10 mM imidazole) and bound proteins eluted with Ni Elution Buffer (50 mM Tris pH 8.0, 300 mM NaCl, 250 mM imidazole). The His-tag was cleaved using TEV protease.

For nanodisc reconstitution, a protocol was adapted from Gao *et al*[60]. The lipids were prepared by resuspending 2.5 mg of lipid powder in 1 ml of chloroform in a glass test tube. The chloroform was then evaporated slowly under argon gas, to produce a thin film of lipids on the bottom of the tube, and further left to dry in a vacuum pump for at least 2 hours. The lipids were then resuspended in 200 ul of lipid resuspension buffer (20 mM HEPES, 150 mM NaCl, 14 mM DDM, pH 7.4) and sonicated until the mixture was almost clear. The lipids, MSP1D1 and MlaFEDB were mixed at a molar ratio of 400:4:1, respectively, in nanodisc buffer (20 mM HEPES, 150 mM NaCl, pH 7.4), and left to incubate on ice for 30 mins. Bio beads were added (20 mg per 1 ml nanodisc mixture) and incubated for 1 hour, rocking at 4 °C. A second batch of biobeads were added and incubated at 4 °C overnight. The following day, the biobeads were removed and the sample separated on a Superdex 200 16/60 gel filtration column (GE Healthcare) equilibrated in nanodisc buffer (20 mM HEPES, 150 mM NaCl, pH 7.4). The appropriate fractions were assessed by SDS PAGE and negative stain EM, and were pooled and concentrated for cryo-EM grid preparation.

Cryo-EM grid preparation and data collection

After size exclusion chromatography, 3 µL of MlaFEDB reconstituted into nanodiscs (at a final concentration of 0.95 mg/mL) was applied to 400 mesh quantifoil holey carbon grids 1.2/1.3. The sample was then frozen in liquid ethane using the Vitrobot Mark III. Pre-screening of the grids was performed on Arcticas equipped with K2 cameras, operated at 200 kV, and located at PNCC (Portland, OR) or at NYU (New York, NY). Acquisition of the movies used for the final reconstruction was performed on a Titan Krios microscope ("Krios 2") equipped with Gatan K2 Summit camera controlled via Leginon[61] and operated at 300 kV (located at the New York Structural Biology Center, NY). Image stacks of 30 frames were collected in super-resolution mode at 0.416 Å per pixel. Data collection parameters are shown in **Supplementary Table S1**.

Cryo-EM data processing

The overall strategy is summarized in supplemental **Fig. S1**. The initial preprocessing steps were all performed within Relion 2.1[62,63]. Movies were drift corrected with MotionCor2[64] and CTF estimation was performed using GCTF[65]. ~1,000 particles were selected manually and subjected to 2D classification. The resulting class averages were used as templates for subsequent automated particle picking of 1,283,606 particles that were extracted with a box size of 300 pixels. The data was then exported in CryoSparc v 0.6[66] for further processing. After 2D classification, 731,205 particles were used to generate an ab-initio model subjected to heterogenous refinement of 3 classes. The 3rd class led to a reasonable map with the shape and size previously published[29]. A second round of heterogeneous classification was then run with the 376,885 particles from this class: only class 3 led to a high resolution map from 209,224 particles. A curation step was applied to only include particles with assignment probability greater than a threshold of 0.95, reducing the number of particles to 177,513. Particles were then imported back to Relion for additional rounds of local refinement after having re-extracted the particles with a 500 pixel box size. In Relion 3.1-beta, we performed local CTF and aberration refinement and then performed particle polishing (re-doing first motion correction with Relion's own implementation of MotionCorr), which improved the resolution from ~3.5 Å to ~3.3 Å. A second round of CTF and aberration refinement further improved the resolution to ~3.2 Å. The data was then imported into CryoSparc 2.12 for another round of refinement to 3.05 Å (some default parameters were modified: we used 3 extra final passes instead of 1, a batchsize epsilon of 0.0005, set the "optimize per particle defocus" and "per group ctf parameters" options to true). Average resolution was estimated using gold standard methods and implementations within Relion and Cryosparc.

Other data processing strategies were explored but failed to bring additional information or improve the resolution: signal subtraction and focused refinement of subdomains (of MlaE, or MlaFEB with and without C2 symmetry), other rounds of 3D classification, further restrict the selection of particles to the best ones relying on the probability distributions computed in Relion (rlnLogLikeliContribution rlnMaxValueProbabilityDistribution). To assess whether the two lipid densities were coming from different proteins averaged in a single map, we also performed various focused 3D classification with variable masks and regularization parameters but this didn't result in clear structures having only one of the two lipids, showing that the two of them are indeed likely present in the pocket at the same time. Transfer of data from CryoSparc to Relion was performed using pyem[67].

Model building

The following models were used as a starting models for the MlaFEDB structure: for MlaFB, the X-Ray structure[35]; for the MCE domain protein MlaD, PDB ID: 5UW2[29]; and for MlaE, a computationally predicted model[29]. Domains were docked as rigid bodies in Chimera[68], and manual model building was

done in COOT[69]. The models were then iteratively refined using the real_space_refine algorithm in PHENIX[70,71], with rounds of manual model building in between using COOT. Some, but not all, of the flexible loops (residues 119-125) that were not modeled in the original X-Ray structure could be traced in our EM map. The 6 TM helices, not present in the construct used of the X-Ray structure, were built *de novo*. For the helices contacting TM2 and TM3 of MlaE ($TM^{A/D}$), side chain density is clearly visible. For the helices contacting IF1 of MlaE further away from the N-Terminus ($TM^{B/E}$), side-chain residues could also be seen and modelled with confidence. Interestingly, on one side of the MlaE dimer, the two MlaD TM helices contacting IF1 were almost fully resolved, while on the other side of the dimer, side-chain residues could only be seen near the contact with the IF1 helix, leading to helix TM^{B} missing the top 6 residues. For the helices contacting IF1 of MlaE near the N-Terminus ($TM^{C/F}$), the EM map was filtered to 6 Å to better visualize the density, these helices are more flexible. Gly11 of MlaD-$TM^{B/E}$ and residues IF1 are part of a larger interaction motif (17-LxxFGxxxL-25) (**Fig. S5a**). MlaD-$TM^{C/F}$ interact with IF1 in a similar manner in the vicinity of MlaE Gly10, which is part of a very similar motif (6-LxxLGxxxI-14). While density for side chains in MlaD $TM^{C/F}$ is weak, the similarity in helix packing geometry and these two binding sites, along with only one available Gly for close helix packing in the MlaD TM helix suggest that the same surface of the MlaD TM is used for IF1 binding in these chains C and F as well. Consequently, we have used this Gly-Gly close packing to establish a likely sequence register for these TM helices. Due to the lower resolution, we have stubbed the side chains of these residues. The loops between the TM helices and the MCE domains of MlaD could not be resolved (5-8 residues missing). Like in the X-Ray structure, the C-terminus of MlaD could also not be resolved (residues 153-183 missing).

The MlaE region displayed the highest local resolution (below 3 Å in its core) and was almost entirely modelled. The two most flexible regions were the extremities of the interfacial helices IF1 (the N-Terminus and the connection to the TM1 helix). Due to a lack of density on the N-terminus of IF1, residues 1-4 could not be modelled. Within the MlaE dimer and at the interface with MlaD, we identified two clearly defined densities that corresponded to the shape and size of phospholipids, which are present in our reconstitution. Phosphatidylethanolamine molecules (code: PEF) were obtained from the Monomer Library in Coot and manually placed into the densities. The phosphate atom could be clearly placed but the ethanolamine portion of the head group was removed due to a lack of density. Using both the high resolution map and its filtered version at 6Å, we also modelled both coils of the membrane scaffold protein belt surrounding the edges of the nanodisc (starting with the ones modelled in PDB: 6CM1). Due to the low resolution, their position is modeled as a poly-alanine helix. Surprisingly, the nanodisc in our sample is unexpectedly small, and we model only ~160 residues.

Structure analysis and Bioinformatics

As structural deviations between MlaE and other type II exporters made database searches more difficult, we conducted a Dali search[72] initiated with MlaF to recover all of the PDB structures containing an ABC domain. These structures were then manually curated based upon the presence or absence of TMDs and further classified based upon the TMD fold.

In order to assess the conservation of MlaD and MlaE sequences across species, we identified at least one “representative” species from each major bacterial order, across the entire bacterial kingdom. Within each order, we selected “representative” species based upon a subjective assessment of their biomedical relevance (prior to an examination of the sequences, to avoid bias). For each representative species, we search the reference genome using BLAST to identify possible homologs of *E. coli* MlaE, MlaD, MlaC, and MlaA. We did not search directly for MlaF or MlaB homologs, as ABC ATPases and STAS domain proteins unrelated to Mla are common in bacteria. Of 92 species analyzed, only 13 were determined to encode what appeared to be functional MCE transporters that were “true homologs” of Mla. To be included in this group, the species must encode a homolog of MlaD (single MCE domain without a long C-terminal helical region (less than ~50 residues) and also homologs of MlaE, MlaC, and MlaA in its genome. In every case, MlaE, MlaD, and MlaC were encoded just downstream of an MlaF-like ABC subunit, and just upstream of an MlaB-like protein (except in Rickettsia rickettsii, which appears to lack MlaB). Sometimes MlaA was encoded in the same operon, while sometimes it was encoded elsewhere in the genome. The resulting “True Mla” homologs were subsequently used for sequence analysis. Sequence alignments were generated using MUSCLE[73] and visualized using JalView[74].

The 3DFSC in **Supplementary Table S2** was measured using the Remote 3DFSC Processing Server[75]. The interfaces between the different subunits of MlaFEDB, Lpt and ABCA/G proteins were analyzed using the COCOMAPS server[76]. The area of the cavities of MlaE and LptFG were estimated using CASTp[55] and HOLLOW[77]. The curvature of the IF2-TM1 helices was analyzed

using Bendix[78] and the corresponding figures generated with VMD software support which is developed with NIH support by the Theoretical and Computational Biophysics group at the Beckman Institute, University of Illinois at Urbana-Champaign. All other figures were made with Chimera[68] or PyMOL (Schrödinger, LLC). The PyMOL plugin, anglebetweenhelices (Schrödinger, LLC), was used to compute the angle between IF1 of MlaE and the TM helices of MlaD.

***Phenotypic assays for* mla *mutants in* E. coli**

Knockouts of *mlaD* and *mlaE* were constructed in *E. coli* BW25113 by P1 transduction from the Keio collection[79], followed by excision of the antibiotic resistance cassettes using pCP20[80]. Serial dilutions of the strains in 96 well plates were manually spotted (2 uL each), on plates containing LB agar or LB agar supplemented with SDS+EDTA sensitivity was assayed in LB agar supplemented with 0.2% SDS and 0.35 mM EDTA, and incubated overnight at 37 °C. We find that this growth assay is very sensitive to the reagents used, particularly the LB agar (see Kolich *et al*[35]). For the experiments reported here, we used Difco LB agar pre-mix (BD Difco #244510), a 10% stock solution of SDS (Sigma L5750), and a 500 mM stock solution of EDTA, pH 8.0 (Sigma ED2SS).

For complementation and/or testing the functionality of the various MlaD and MlaE mutants, a pBAD-derived plasmid harboring the *mlaFEDCB* operon was transformed into the appropriate knockout strain. To test the functionality of mutations in MlaE, we transformed the *mlaE* knockout strain with pBEL1200 (*mlaFEDCB* operon with N-terminal tag on MlaD, see **Supplementary Table S3**), or derivatives of this plasmid harboring the mutations in MlaE IF1. For the MlaD mutants, we transformed the *mlaD* knockout strain with pBEL1198 (*mlaFEDCB* operon N-terminal tag on MlaE, see **Supplementary Table S3**), or mutant derivatives of the MlaD TM helices. We found that leaky expression from the pBAD promoter was sufficient for complementation of the phenotypes of both the *mlaD* and *mlaE* knockout strains, and thus no L-arabinose was added.

Western blot to detect MlaD TM mutants

In order to assess the expression and cellular localisation of the MlaD TM mutant, each of the pBEL1198 derived plasmids were expressed and purified as described above (see **Expression and purification of MlaFEDB**). Following cell lysis and a low speed spin to remove cell debris, a sample was collected, which we refer to as the “whole cell lysate”. The membranes were then isolated and solubilized as described above, and a sample was taken from the solubilized membranes, which we refer to as the “membrane fraction”. 10 µl of each sample were separated on an SDS-PAGE gel and transferred to a nitrocellulose membrane. The membranes were blocked in PBST containing 5% milk for 1 hour. The membranes were then incubated with primary antibody (rabbit polyclonal anti-MlaD at a dilution of 1:10000) in PBST + 5% milk overnight at 4 °C. The membranes were then washed 3 times with PBST and were incubated with anti-rabbit HRP conjugated secondary antibody (GE Healthcare, #NA934) in PBST + 5% milk for 1 hour. The membranes were then washed 3 times with PBST and incubated with ECL (Thermo Fisher Scientific, #32109) substrate and developed using autoradiography film (Denville, #B07TD14PXW).

Lipid crosslinking experiments

This method was adapted from Isom and Coudray *et al*, 2020[56]. T7express *E. coli* (NEB) were co-transformed with plasmids to express MlaFEDCB (either WT or mutant forms derived from pBEL1198) and pEVOL-pBpF (Addgene #31190), which encodes a tRNA synthetase/tRNA pair for the *in vivo* incorporation p-benzoyl-l-phenylalanine (BPA) in *E. coli* proteins at the amber stop codon, TAG[31,57]. Bacterial colonies were inoculated in LB broth supplemented with carbenicillin (100 µg/mL) and chloramphenicol (38 µg/mL) and grown overnight at 37 °C. The following day, bacteria were pelleted and resuspended in ^{32}P Labelling Medium (a low phosphate minimal media: 1 mM Na2HP04, 1 mM KH2PO4, 50 mM NH4Cl, 5 mM Na2SO4, 2 mM MgSO4, 20 mM Na2-Succinate, 0.2x trace metals and 0.2% glucose) supplemented with carbenicillin (100 µg/mL) and chloramphenicol (38 µg/mL) and inoculated 1:50 in the 10 ml of the same medium. Bacteria were grown to OD 0.9 and a final concentration of 0.2% L-arabinose and 0.5 mM BPA (Bachem, #F-2800.0005), alongside 500 µCi ^{32}P orthophosphoric acid (PerkinElmer, #NEX053010MC) were added and left to induce overnight.

The following day, the cultures were spun down and resuspended in 500 µl of lysozyme-EDTA resuspension buffer (50 mM Tris pH 8.0, 300 mM NaCl, 10 mM imidazole, 1 mg/ml lysozyme, 0.5 mM EDTA, 25U benzonase) and were incubated for 1 hour at room temperature. The samples then underwent crosslinking by treatment with 365 nM UV in a Spectrolinker for 30 mins. For lysis, the crosslinked samples were added to 250 µl of 100 mM DDM, and 0.48 g of urea, and adjusted up to a total volume of 1 ml using 10 mM wash buffer (50 mM Tris pH 8.0, 300 mM NaCl, 10 mM imidazole), and incubated at 60 °C, with intermittent inversion of the tubes to mix, until the urea was dissolved and the cells had undergone lysis (approximately 15

mins). Each sample was then mixed with 25 µl of nickel beads (Ni Sepharose 6 Fast Flow) for 30 mins. The beads were pelleted at 500 xg for 1 min and the supernatant collected. The beads were then washed four times with urea wash buffer (50 mM Tris pH 8.0, 300 mM NaCl, 40 mM imidazole, 8M urea, 0.5 mM DDM) and finally resuspended in 50 µl of urea wash buffer (50 mM Tris pH 8.0, 300 mM NaCl, 250 mM imidazole, 8M urea, 0.5 mM DDM). The samples were then mixed with 5x SDS-PAGE loading buffer, and the beads spun down at 12,000 xg for 2 mins. Eluted protein was analyzed by SDS-PAGE and stained using InstantBlue™ Protein Stain (Expedeon, #isb1l). Relative MlaE loading on the gel was estimated integrating the density of the corresponding bands in the InstantBlue-stained gel in ImageJ[81], and this was used to normalize the amount of MlaE loaded on a second gel, to enable more accurate comparisons between samples. The normalized gel was stained and ^{32}P signal was detected using a phosphor screen and scanned on a Typhoon scanner (Amersham). Three replicates of the experiment were performed, starting with protein expression.

Western blots to detect monomeric and dimeric MlaE in crosslinked samples

The WT and mutant forms of MlaE (derived from pBEL1198), were expressed and purified as described above (in **Lipid crosslinking experiments**), but in the absence of ^{32}P ortho-phosphoric acid. The western blot was done as described above (in **Western blots to detect MlaD TM mutants**), but with an anti-his antibody (Qiagen, #34660) as primary, to detect his-tagged MlaE, and HRP-linked anti-mouse (GE Healthcare, #NA931-1ML) as the secondary antibody.

Acknowledgments

We thank Marisa Lopez-Redondo (NYU) and Yuan Gao (UCSF) for guidance with nanodisc reconstitution, and members of the Bhabha/Ekiert labs for helpful discussions. We thank Ian Henderson (University of Queensland) for providing anti-MlaD antibodies. We gratefully acknowledge the following funding sources: NIH grant R35GM128777 (D.C.E.), NIH grant R00GM112982, Damon Runyon Cancer Research Foundation grant DFS-20-16 and Pew Charitable Trusts PEW-00033055 (G.B.). American Heart Association postdoctoral fellowship 20POST35210202 (G.L.I), NIH T32 predoctoral training grant T32 GM088118 (M.R.M). Pre-screening was done at the NYU cryo-EM core facility of and the Pacific Northwest Center for Cryo EM. CryoEM data were collected at the Simons Electron Microscopy Center and National Resource for Automated Molecular Microscopy located at the New York Structural Biology Center, supported by grants from the Simons Foundation (SF349247), NYSTAR, and the NIH National Institute of General Medical Sciences (GM103310) with additional support from Agouron Institute (F00316) and NIH (OD019994). A portion of this research was supported by NIH grant U24GM129547 and performed at the Pacific Northwest Center for Cryo- EM at Oregon Health & Sciences University (OHSU) and accessed through EMSL (grid.436923.9), a DOE Office of Science User Facility sponsored by the Office of Biological and Environmental Research. EM data processing has utilized computing resources at the HPC Facility at NYU, and we thank the HPC team. Molecular graphics and analyses performed with UCSF Chimera, developed by the Resource for Biocomputing, Visualization, and Informatics at the University of California, San Francisco, with support from NIH P41-GM103311.

Author contributions

G.L.I, M.R.M., N.C., G.B. and D.C.E. conceived the study. G.L.I, M.R.M, N.C. and M.S. carried out the experiments. G.L.I, M.R.M., N.C., G.B. and D.C.E. analyzed the data. G.L.I, M.R.M., N.C., G.B. and D.C.E. wrote the manuscript with contributions from all other authors.

Competing Interests Statement

The authors declare no competing interests.

References

1. Juliano, R. L. & Ling, V. A surface glycoprotein modulating drug permeability in Chinese hamster ovary cell mutants. *Biochim. Biophys. Acta* **455**, 152–162 (1976).
2. Jackson, S. M. *et al.* Structural basis of small-molecule inhibition of human multidrug transporter ABCG2. *Nat. Struct. Mol. Biol.* **25**, 333–340 (2018).
3. Fitzpatrick, A. W. P. *et al.* Structure of the MacAB-TolC ABC-type tripartite multidrug efflux pump. *Nat Microbiol* **2**, 17070 (2017).
4. Polissi, A. & Georgopoulos, C. Mutational analysis and properties of the msbA gene of Escherichia coli, coding for an essential ABC family transporter. *Mol. Microbiol.* **20**, 1221–1233 (1996).
5. Brooks-Wilson, A. *et al.* Mutations in ABC1 in Tangier disease and familial high-density lipoprotein deficiency. *Nat. Genet.* **22**, 336–345 (1999).
6. Bodzioch, M. *et al.* The gene encoding ATP-binding cassette transporter 1 is mutated in

Tangier disease. *Nat. Genet.* **22**, 347–351 (1999).
7. Rust, S. *et al.* Tangier disease is caused by mutations in the gene encoding ATP-binding cassette transporter 1. *Nat. Genet.* **22**, 352–355 (1999).
8. Berge, K. E. Accumulation of Dietary Cholesterol in Sitosterolemia Caused by Mutations in Adjacent ABC Transporters. *Science* vol. 290 1771–1775 (2000).
9. Mi, W. *et al.* Structural basis of MsbA-mediated lipopolysaccharide transport. *Nature* **549**, 233–237 (2017).
10. Padayatti, P. S. *et al.* Structural Insights into the Lipid A Transport Pathway in MsbA. *Structure* **27**, 1114–1123.e3 (2019).
11. Ward, A., Reyes, C. L., Yu, J., Roth, C. B. & Chang, G. Flexibility in the ABC transporter MsbA: Alternating access with a twist. *Proc. Natl. Acad. Sci. U. S. A.* **104**, 19005–19010 (2007).
12. Li, Y., Orlando, B. J. & Liao, M. Structural basis of lipopolysaccharide extraction by the LptB2FGC complex. *Nature* vol. 567 486–490 (2019).
13. Botos, I. *et al.* Structural and Functional Characterization of the LPS Transporter LptDE from Gram-Negative Pathogens. *Structure* **24**, 965–976 (2016).
14. Owens, T. W. *et al.* Structural basis of unidirectional export of lipopolysaccharide to the cell surface. *Nature* **567**, 550–553 (2019).
15. Suits, M. D. L., Sperandeo, P., Dehò, G., Polissi, A. & Jia, Z. Novel structure of the conserved gram-negative lipopolysaccharide transport protein A and mutagenesis analysis. *J. Mol. Biol.* **380**, 476–488 (2008).
16. Dong, H. *et al.* Structural basis for outer membrane lipopolysaccharide insertion. *Nature* **511**, 52–56 (2014).
17. Qiao, S., Luo, Q., Zhao, Y., Zhang, X. C. & Huang, Y. Structural basis for lipopolysaccharide insertion in the bacterial outer membrane. *Nature* vol. 511 108–111 (2014).
18. Malojčić, G. *et al.* LptE binds to and alters the physical state of LPS to catalyze its assembly at the cell surface. *Proc. Natl. Acad. Sci. U. S. A.* **111**, 9467–9472 (2014).
19. Ho, H. *et al.* Structural basis for dual-mode inhibition of the ABC transporter MsbA. *Nature* **557**, 196–201 (2018).
20. Martin-Loeches, I., Dale, G. E. & Torres, A. Murepavadin: a new antibiotic class in the pipeline. *Expert Rev. Anti. Infect. Ther.* **16**, 259–268 (2018).
21. Storek, K. M. *et al.* Massive antibody discovery used to probe structure–function relationships of the essential outer membrane protein LptD. *Elife* **8**, e46258 (2019).
22. Malinverni, J. C. & Silhavy, T. J. An ABC transport system that maintains lipid asymmetry in the gram-negative outer membrane. *Proc. Natl. Acad. Sci. U. S. A.* **106**, 8009–8014 (2009).
23. Shrivastava, R. & Chng, S.-S. Lipid trafficking across the Gram-negative cell envelope. *Journal of Biological Chemistry* vol. 294 14175–14184 (2019).
24. Hughes, G. W. *et al.* Evidence for phospholipid export from the bacterial inner membrane by the Mla ABC transport system. *Nat Microbiol* **4**, 1692–1705 (2019).
25. Kamischke, C. *et al.* The Acinetobacter baumannii Mla system and glycerophospholipid transport to the outer membrane. *eLife* vol. 8 (2019).
26. Ercan, B., Low, W.-Y., Liu, X. & Chng, S.-S. Characterization of Interactions and Phospholipid Transfer between Substrate Binding Proteins of the OmpC-Mla System. *Biochemistry* **58**, 114–119 (2019).
27. Yeow, J. *et al.* The architecture of the OmpC–MlaA complex sheds light on the maintenance of outer membrane lipid asymmetry inEscherichia coli. *Journal of Biological Chemistry* vol. 293 11325–11340 (2018).
28. Abellón-Ruiz, J. *et al.* Structural basis for maintenance of bacterial outer membrane lipid asymmetry. *Nat Microbiol* **2**, 1616–1623 (2017).
29. Ekiert, D. C. *et al.* Architectures of Lipid Transport Systems for the Bacterial Outer Membrane. *Cell* **169**, 273–285.e17 (2017).
30. Powers, M. J. & Trent, M. S. Phospholipid retention in the absence of asymmetry strengthens the outer membrane permeability barrier to last-resort antibiotics. *Proc. Natl. Acad. Sci. U. S. A.* **115**, E8518–E8527 (2018).
31. Isom, G. L. *et al.* MCE domain proteins: conserved inner membrane lipid-binding proteins required for outer membrane homeostasis. *Sci. Rep.* **7**, 8608 (2017).
32. Chong, Z.-S., Woo, W.-F. & Chng, S.-S. Osmoporin OmpC forms a complex with MlaA to maintain outer membrane lipid asymmetry in Escherichia coli. *Mol. Microbiol.* **98**, 1133–1146 (2015).
33. Thong, S. *et al.* Defining key roles for auxiliary proteins in an ABC transporter that maintains bacterial outer membrane lipid asymmetry. *Elife* **5**, (2016).
34. Shrivastava, R., Jiang, X. 'er & Chng, S.-S. Outer membrane lipid homeostasis via retrograde phospholipid transport in Escherichia coli. *Mol. Microbiol.* **106**, 395–408

(2017).
35. Kolich, L. *et al.* Structure of MlaFB uncovers novel mechanisms of ABC transporter regulation. *bioRxiv* (2000) doi:10.1101/2020.04.27.064196.
36. Lee, J.-Y. *et al.* Crystal structure of the human sterol transporter ABCG5/ABCG8. *Nature* **533**, 561–564 (2016).
37. Murakami, S., Okada, U. & Yamashita, E. Crystal structure of tripartite-type ABC transporter, MacB from Acinetobacter baumannii. (2017) doi:10.2210/pdb5gko/pdb.
38. Bayburt, T. H., Grinkova, Y. V. & Sligar, S. G. Self-Assembly of Discoidal Phospholipid Bilayer Nanoparticles with Membrane Scaffold Proteins. *Nano Lett.* **2**, 853–856 (2002).
39. Karpowich, N. *et al.* Crystal structures of the MJ1267 ATP binding cassette reveal an induced-fit effect at the ATPase active site of an ABC transporter. *Structure* **9**, 571–586 (2001).
40. Smith, P. C. *et al.* ATP binding to the motor domain from an ABC transporter drives formation of a nucleotide sandwich dimer. *Mol. Cell* **10**, 139–149 (2002).
41. Orelle, C. *et al.* Dynamics of α-helical subdomain rotation in the intact maltose ATP-binding cassette transporter. *Proc. Natl. Acad. Sci. U. S. A.* **107**, 20293–20298 (2010).
42. Chen, L. *et al.* Cryo-electron Microscopy Structure and Transport Mechanism of a Wall Teichoic Acid ABC Transporter. *mBio* vol. 11 (2020).
43. Luo, Q. *et al.* Structural basis for lipopolysaccharide extraction by ABC transporter LptBFG. *Nat. Struct. Mol. Biol.* **24**, 469–474 (2017).
44. Bi, Y., Mann, E., Whitfield, C. & Zimmer, J. Architecture of a channel-forming O-antigen polysaccharide ABC transporter. *Nature* **553**, 361–365 (2018).
45. Tang, X. *et al.* Cryo-EM structures of lipopolysaccharide transporter LptB2FGC in lipopolysaccharide or AMP-PNP-bound states reveal its transport mechanism. *Nature Communications* vol. 10 (2019).
46. Dong, H., Zhang, Z., Tang, X., Paterson, N. G. & Dong, C. Structural and functional insights into the lipopolysaccharide ABC transporter LptB2FG. *Nature Communications* vol. 8 (2017).
47. Caffalette, C. A., Corey, R. A., Sansom, M. S. P., Stansfeld, P. J. & Zimmer, J. A lipid gating mechanism for the channel-forming O antigen ABC transporter. *Nat. Commun.* **10**, 824 (2019).
48. Qian, H. *et al.* Structure of the Human Lipid Exporter ABCA1. *Cell* **169**, 1228–1239.e10 (2017).
49. Orlando, B. J. & Liao, M. ABCG2 transports anticancer drugs via a closed-to-open switch. *Nature Communications* vol. 11 (2020).
50. Manolaridis, I. *et al.* Cryo-EM structures of a human ABCG2 mutant trapped in ATP-bound and substrate-bound states. *Nature* **563**, 426–430 (2018).
51. Kadaba, N. S., Kaiser, J. T., Johnson, E., Lee, A. & Rees, D. C. The high-affinity E. coli methionine ABC transporter: structure and allosteric regulation. *Science* **321**, 250–253 (2008).
52. Gerber, S., Comellas-Bigler, M., Goetz, B. A. & Locher, K. P. Structural basis of trans-inhibition in a molybdate/tungstate ABC transporter. *Science* **321**, 246–250 (2008).
53. Aller, S. G. *et al.* Structure of P-glycoprotein reveals a molecular basis for poly-specific drug binding. *Science* **323**, 1718–1722 (2009).
54. Li, Y., Orlando, B. J. & Liao, M. Structural basis of lipopolysaccharide extraction by the LptBFGC complex. *Nature* **567**, 486–490 (2019).
55. Tian, W., Chen, C., Lei, X., Zhao, J. & Liang, J. CASTp 3.0: computed atlas of surface topography of proteins. *Nucleic Acids Res.* **46**, W363–W367 (2018).
56. Isom, G. L. *et al.* LetB Structure Reveals a Tunnel for Lipid Transport across the Bacterial Envelope. *Cell* **181**, 653–664.e19 (2020).
57. Chin, J. W., Martin, A. B., King, D. S., Wang, L. & Schultz, P. G. Addition of a photocrosslinking amino acid to the genetic code of Escherichia coli. *Proceedings of the National Academy of Sciences* vol. 99 11020–11024 (2002).
58. Doerrler, W. T. & Raetz, C. R. H. ATPase Activity of the MsbA Lipid Flippase ofEscherichia coli. *Journal of Biological Chemistry* vol. 277 36697–36705 (2002).
59. Eckford, P. D. W. & Sharom, F. J. The reconstituted Escherichia coli MsbA protein displays lipid flippase activity. *Biochemical Journal* vol. 429 195–203 (2010).
60. Gao, Y., Cao, E., Julius, D. & Cheng, Y. TRPV1 structures in nanodiscs reveal mechanisms of ligand and lipid action. *Nature* **534**, 347–351 (2016).
61. Suloway, C. *et al.* Automated molecular microscopy: the new Leginon system. *J. Struct. Biol.* **151**, 41–60 (2005).
62. Fernandez-Leiro, R. & Scheres, S. H. W. A pipeline approach to single-particle processing in RELION. *Acta Crystallogr D Struct Biol* **73**, 496–502 (2017).
63. Kimanius, D., Forsberg, B. O., Scheres, S. H. & Lindahl, E. Accelerated cryo-EM structure determination with parallelisation using GPUs

in RELION-2. *Elife* **5**, (2016).
64. Zheng, S. Q. *et al.* MotionCor2: anisotropic correction of beam-induced motion for improved cryo-electron microscopy. *Nature Methods* vol. 14 331–332 (2017).
65. Zhang, K. Gctf: Real-time CTF determination and correction. *Journal of Structural Biology* vol. 193 1–12 (2016).
66. Punjani, A., Rubinstein, J. L., Fleet, D. J. & Brubaker, M. A. cryoSPARC: algorithms for rapid unsupervised cryo-EM structure determination. *Nat. Methods* **14**, 290–296 (2017).
67. Asarnow, D., Palovcak, E., Cheng, Y. UCSF pyem. *UCSF pyem v0.5* https://doi.org/10.5281/zenodo.3576630 (2019) doi:10.5281/zenodo.3576630.
68. Pettersen, E. F. *et al.* UCSF Chimera--a visualization system for exploratory research and analysis. *J. Comput. Chem.* **25**, 1605–1612 (2004).
69. Emsley, P., Lohkamp, B., Scott, W. G. & Cowtan, K. Features and development of Coot. *Acta Crystallogr. D Biol. Crystallogr.* **66**, 486–501 (2010).
70. Echols, N. *et al.* Graphical tools for macromolecular crystallography in PHENIX. *J. Appl. Crystallogr.* **45**, 581–586 (2012).
71. Adams, P. D. *et al.* PHENIX: a comprehensive Python-based system for macromolecular structure solution. *Acta Crystallogr. D Biol. Crystallogr.* **66**, 213–221 (2010).
72. Holm, L. Benchmarking fold detection by DaliLite v.5. *Bioinformatics* **35**, 5326–5327 (2019).
73. Edgar, R. C. MUSCLE: multiple sequence alignment with high accuracy and high throughput. *Nucleic Acids Research* vol. 32 1792–1797 (2004).
74. Waterhouse, A. M., Procter, J. B., Martin, D. M. A., Clamp, M. & Barton, G. J. Jalview Version 2--a multiple sequence alignment editor and analysis workbench. *Bioinformatics* vol. 25 1189–1191 (2009).
75. Tan, Y. Z. *et al.* Addressing preferred specimen orientation in single-particle cryo-EM through tilting. *Nat. Methods* **14**, 793–796 (2017).
76. Vangone, A., Spinelli, R., Scarano, V., Cavallo, L. & Oliva, R. COCOMAPS: a web application to analyze and visualize contacts at the interface of biomolecular complexes. *Bioinformatics* **27**, 2915–2916 (2011).
77. Ho, B. K. & Gruswitz, F. HOLLOW: generating accurate representations of channel and interior surfaces in molecular structures. *BMC Struct. Biol.* **8**, 49 (2008).
78. Dahl, A. C. E., Chavent, M. & Sansom, M. S. P. Bendix: intuitive helix geometry analysis and abstraction. *Bioinformatics* **28**, 2193–2194 (2012).
79. Baba, T. *et al.* Construction of Escherichia coli K-12 in-frame, single-gene knockout mutants: the Keio collection. *Mol. Syst. Biol.* **2**, 2006.0008 (2006).
80. Cherepanov, P. P. & Wackernagel, W. Gene disruption in Escherichia coli: TcR and KmR cassettes with the option of Flp-catalyzed excision of the antibiotic-resistance determinant. *Gene* vol. 158 9–14 (1995).
81. Rueden, C. T. *et al.* ImageJ2: ImageJ for the next generation of scientific image data. *BMC Bioinformatics* **18**, 529 (2017).